

## Quadrupole moment of $^{203}\text{Fr}$

S. G. Wilkins,<sup>1,\*</sup> K. M. Lynch,<sup>2</sup> J. Billowes,<sup>1</sup> C. L. Binnersley,<sup>1</sup> M. L. Bissell,<sup>1</sup> T. E. Cocolios,<sup>3</sup> T. Day Goodacre,<sup>1,4,†</sup>  
 R. P. de Groote,<sup>3</sup> G. J. Farooq-Smith,<sup>3</sup> K. T. Flanagan,<sup>1</sup> S. Franchoo,<sup>5</sup> R. F. Garcia Ruiz,<sup>1,3</sup> W. Gins,<sup>3</sup> H. Heylen,<sup>3</sup>  
 Á. Kozsiorús,<sup>3</sup> G. Neyens,<sup>3</sup> H. H. Stroke,<sup>6</sup> A. R. Vernon,<sup>1</sup> K. D. A. Wendt,<sup>7</sup> and X. F. Yang<sup>3</sup>

<sup>1</sup>*School of Physics and Astronomy, The University of Manchester, Manchester M13 9PL, UK*

<sup>2</sup>*ISOLDE, EP Department, CERN, CH-1211 Geneva 23, Switzerland*

<sup>3</sup>*KU Leuven, Instituut voor Kern- en Stralingsfysica, Celestijnenlaan 200D, 3001 Leuven, Belgium*

<sup>4</sup>*EN Department, CERN, CH-1211 Geneva 23, Switzerland*

<sup>5</sup>*Institut de Physique Nucléaire d'Orsay, F-91406 Orsay, France*

<sup>6</sup>*Department of Physics, New York University, New York, New York 10003, USA*

<sup>7</sup>*Institut für Physik, Johannes Gutenberg-Universität, D-55128 Mainz, Germany*

(Received 30 June 2017; revised manuscript received 17 August 2017; published 19 September 2017)

The spectroscopic electric quadrupole moment of the neutron-deficient francium isotope  $^{203}\text{Fr}$  was measured by using high-resolution collinear resonance ionization spectroscopy (CRIS) at the CERN Isotope Separation On-Line Device (ISOLDE) facility. A remeasurement of the  $^{207}\text{Fr}$  quadrupole moment was also performed, resulting in a departure from the established literature value. A sudden increase in magnitude of the  $^{203}\text{Fr}$  quadrupole moment, with respect to the general trend in the region, points to an onset of static deformation at  $N = 116$  in the  $_{87}\text{Fr}$  isotopic chain. Calculation of the static and total deformation parameters show that the increase in static deformation only cannot account for the observed departure of its relative charge radius from the  $_{82}\text{Pb}$  chain.

DOI: [10.1103/PhysRevC.96.034317](https://doi.org/10.1103/PhysRevC.96.034317)

### I. INTRODUCTION

Neutron-deficient isotopes in the vicinity of the  $Z = 82$  and  $N = 126$  shell closures have been the subject of continued experimental and theoretical interest. Low-lying states with shape configurations that differ from the ground state lead to shape coexistence in the region [1]. For odd- $Z$ , even- $N$  nuclei above  $Z = 82$  and below  $N = 126$ , a competition arises between the spherical  $\pi 1h_{9/2}$  ground state and oblate  $\pi 3s_{1/2}$  intruder state. The excitation energy of this intruder state decreases as the neutron orbitals below  $N = 126$  are depleted. This state inverts with the  $\pi 1h_{9/2}$  state to become the ground state in  $^{185}\text{Bi}$  [2] and  $^{195}\text{At}$  [3]. In  $_{87}\text{Fr}$ , it is predicted to become the ground state in  $^{199}\text{Fr}$  [4–7].

In-source laser spectroscopy studies on the neutron-deficient  $^{193,195,197}\text{Bi}$  isotopes support the previous suggestions of shape-coexistence between a nearly spherical ground state and a deformed intruder isomer [8]: the relative charge radii of these  $_{83}\text{Bi}$  ground states are identical to those of their corresponding lead isotones, which were found to be spherical [9]. The isomeric  $\pi 3s_{1/2}$  intruder states, however, possess a large isomer shift, suggesting that these states are significantly deformed. Spectroscopic quadrupole moments, which can only be measured for states with  $I > 1/2$ , provide a more

direct observable for measuring static deformation. High-precision quadrupole moments of the ground states are only available down to  $N = 120$  in  $_{83}\text{Bi}$  [10]. Quadrupole moments measured via in-source laser spectroscopy are available for  $N = 110$ – $114$  but their limited precision does not allow conclusions to be drawn on the possible onset of static deformation.

High-precision quadrupole moments have been measured in the  $_{87}\text{Fr}$  isotopes [11–14], which have been the subject of recent low- and high-resolution laser spectroscopic experiments [15–19]. Earlier relative charge-radii measurements on neutron-deficient  $_{87}\text{Fr}$  isotopes down to  $N = 120$  showed no departure from the lead isotonic radii, despite the presence of five valence protons in the  $\pi 1h_{9/2}$  orbital [13]. Recent low-resolution laser spectroscopy studies measured down to  $N = 115$  and showed a sudden departure from the  $_{82}\text{Pb}$  radii trend from  $^{203}\text{Fr}$  ( $N = 116$ ) downwards [16]. This suggested an onset of deformation in the  $_{87}\text{Fr}$  chain closer to stability than the departures found in the  $_{83}\text{Bi}$  and  $_{84}\text{Po}$  isotope chains, where they occur at  $N = 110$  and  $N = 114$ , respectively [20–22]. High-resolution laser spectroscopy studies of  $_{87}\text{Fr}$  isotopes have been performed down to  $^{204}\text{Fr}$  [11,12,19], but no firm conclusions on the possible onset of static deformation in the ground states have been reported.

In this article, we present the first high-resolution laser spectroscopy study of  $^{203}\text{Fr}$ . The hyperfine structure was measured through the  $7s\ ^2S_{1/2} \rightarrow 8p\ ^2P_{3/2}$  transition ( $23\ 658.31\ \text{cm}^{-1}$ ) by using the collinear resonance ionization spectroscopy (CRIS) experiment at the CERN Isotope Separation On-Line Device (ISOLDE) facility. A remeasurement of the  $^{207}\text{Fr}$  hyperfine structure is also presented, yielding a new quadrupole-moment value that better follows the trend observed in neighboring isotopes. The  $_{87}\text{Fr}$  quadrupole moments down to  $N = 116$  are compared with those of other nuclear ground

\*shane.wilkins@postgrad.manchester.ac.uk

†Present address: TRIUMF, Vancouver, British Columbia, V6T 2A3, Canada.

Published by the American Physical Society under the terms of the [Creative Commons Attribution 4.0 International](https://creativecommons.org/licenses/by/4.0/) license. Further distribution of this work must maintain attribution to the author(s) and the published article's title, journal citation, and DOI.

and isomeric states in trans-lead elements. A similar gradual increase is observed for all elements as the orbitals below  $N = 126$  are depleted, due to an onset of core polarization [23]. The sudden increase at  $^{203}\text{Fr}$  is interpreted as an onset of static deformation at  $N = 116$ . However, this increase cannot fully account for the observed departure of its relative charge radius from the  $_{82}\text{Pb}$  chain [16].

## II. EXPERIMENTAL TECHNIQUE

The francium isotopes of interest were produced at the CERN Isotope Separation On-Line Device (ISOLDE) radioactive beam facility. Protons at 1.4 GeV from the proton synchrotron booster (PSB) impinged upon a thick uranium-carbide target. Francium isotopes were produced through spallation reactions within the target and surface ionized through collisions with a hot (2400 K) transfer line. The  $^{203,207}\text{Fr}$  ions were then mass separated by using the high-resolution separator (HRS) and subsequently injected into the ISCOOL gas-filled radio-frequency cooler buncher [24]. The ions were allowed to accumulate and released at a rate of 100 Hz with a width of 5  $\mu\text{s}$  before being deflected to the CRIS experiment [25].

The bunched francium ion beam was neutralized in flight in a charge-exchange cell filled with potassium vapor (held at 450 K). Any residual ionic component of the beam was electrostatically deflected away. The neutralized bunches then entered an ultrahigh-vacuum interaction region where they were spatially and temporally overlapped with two laser beams. The pressure of the interaction region was maintained at  $2 \times 10^{-8}$  mbar so that nonresonant collisional re-ionization was minimized. When the frequency of the scanning laser was equal to that of an allowed transition between the ground and excited hyperfine states, the francium atoms were resonantly ionized and deflected onto a microchannel plate (MCP) and detected.

The hyperfine structure of the francium isotopes was probed by using the 422 nm  $7s\ ^2S_{1/2} \rightarrow 8p\ ^2P_{3/2}$  transition. An M-Squared SolsTiS continuous-wave titanium-sapphire laser

(pumped by a Lighthouse Photonics Sprout-G 18 W laser) produced light at 844 nm. The wavelength was measured by a HighFinesse WSU2 wavemeter, which was calibrated by using a temperature-stabilized helium-neon laser as a reference. The 844 nm light was externally frequency doubled by using an M-Squared ECD-X frequency doubler [26].

To prevent optically pumping to dark states, the 422 nm light was “chopped” into 100 ns pulses at a rate of 100 Hz by inducing a  $\lambda/2$  polarization change through fast switching of a Pockels cell between 0 kV (off) and +2.4 kV (on) with a Behlke FSWP91-01 fast square-wave pulser. When the Pockels cell was on, the 422 nm light had the necessary polarization to be reflected by a polarizing beam-splitter cube towards another Pockels cell and polarizing beam-splitter cube. Only when both Pockels cells were on would light be reflected towards a 25 m multimode fiber transporting the light to an optical table adjacent to the CRIS beam line. More details can be found in Ref. [14]. The extinction ratio of the two fast-switching setups operating in series exceeded  $1 : 10^5$ . The peak intensity of the chopped pulses was 60% of the intensity of the continuous-wave light entering the fast-switching setup.

A 1064 nm nonresonant step, delayed by 100 ns, was used to ionize the excited francium atoms in the  $8p\ ^2P_{3/2}$  state. The 83.5(1.5) ns lifetime of the  $8p\ ^2P_{3/2}$  [27] state allowed power broadening and lineshape distortion effects to be removed without a loss in efficiency [28]. This light was produced by a Litron LPY 601 50-100 PIV Nd:YAG running at 100 Hz. The timing of the two laser pulses with respect to the atomic bunch was controlled by using a Quantum Composers QC9258 digital delay pulse generator.

## III. RESULTS

The hyperfine structures of the  $7s\ ^2S_{1/2} \rightarrow 8p\ ^2P_{3/2}$  transition in  $^{203,207}\text{Fr}$  are shown in Fig. 1. The frequency of the spectra is plotted relative to the centroid frequency of  $^{221}\text{Fr}$ . However, the isotope  $^{219}\text{Fr}$  was used as a reference throughout the experiment in order to minimize the accumulated radioactivity on the MCP due to its shorter half-life of 20(2) ms

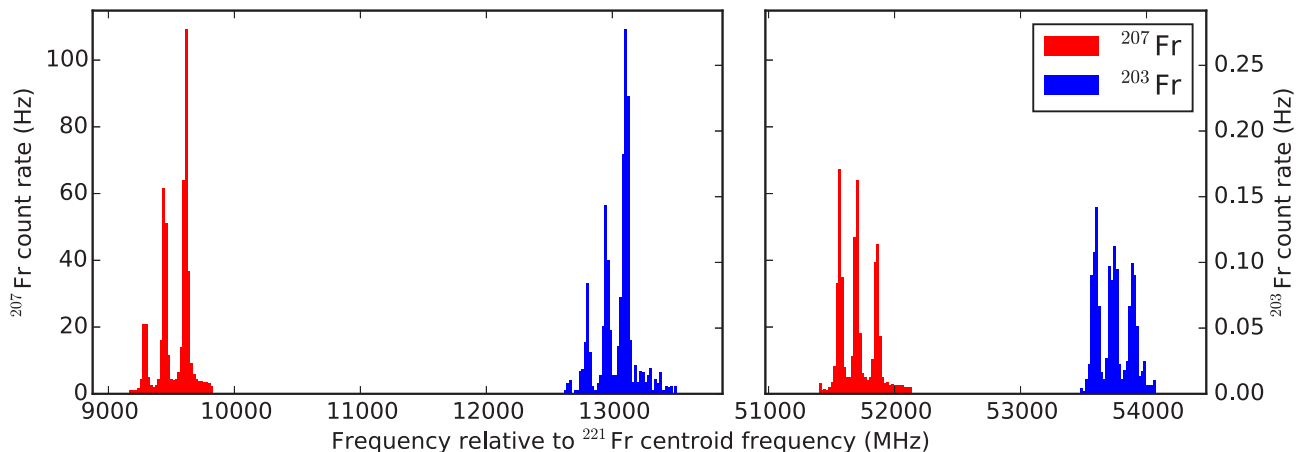


FIG. 1. Hyperfine spectra of  $^{203}\text{Fr}$  (blue) and  $^{207}\text{Fr}$  (red) obtained from collinear resonance ionization spectroscopy, relative to the centroid frequency of  $^{221}\text{Fr}$ .

TABLE I. Spins, hyperfine  $A$  and  $B$  factors, isotope shifts, magnetic dipole moments, spectroscopic quadrupole moments, and changes in mean-square charge radii of  $^{203,207}\text{Fr}$  relative to  $^{221}\text{Fr}$ . The statistical and systematic uncertainties on the changes in mean-square charge radii are given in the first and second sets of brackets, respectively. All hyperfine factors and isotope shifts are given in MHz. Literature values are taken from Refs. [13,16,29]. The quadrupole moments measured through the 717 nm transition were recalculated by using the  $B/Q$  value from Ref. [30]

$I^\pi$	$A$	$A(7s^2S_{1/2})$	$A(8p^2P_{3/2})$	$B(8p^2P_{3/2})$	$\delta\nu^{221,A}$	$\mu$ ( $\mu_N$ )	$Q_s$ (b)	$\delta\langle r^2 \rangle^{221,A}$ ( $\text{fm}^2$ )
203 (expt.)	$9/2^-$	+8187(2)	+29.5(2)	-39.1(20)	+31327(7)	+3.74(4)	-0.47(2)	-1.5302(2)(168)
203 (lit.)	( $9/2^-$ )	+8180(30)			+31320(100)	+3.73(4)		-1.530(18)
207 (expt.)	$9/2^-$	+8482(2)	+30.4(2)	-20.0(16)	+28495(7)	+3.87(4)	-0.24(2)	-1.3897(2)(149)
207 (lit.)	$9/2^-$	+8484(1)			+28420(100)	+3.87(4)	-0.16(5)	-1.386(16)

compared with 4.8 m, as well as a shorter-lived progeny with no isotope along the decay chain with a half-life more than a few minutes. The full width at half maximum (FWHM) of the  $^{203,207}\text{Fr}$  hyperfine peaks was 25 MHz.

The extracted hyperfine  $A$  and  $B$  factors, isotope shifts, spins, magnetic dipole moments, electric quadrupole moments, and changes in the mean-square charge radii for  $^{203,207}\text{Fr}$  are presented in Table I. The isotope shifts are given relative to  $^{221}\text{Fr}$  by using  $\delta\nu^{221,219} = +5475(5)$  MHz in order to compare with our earlier work [15,16]. The magnetic dipole moments were calculated by using the following relation:

$$\mu = \frac{AI}{A_{\text{ref}}I_{\text{ref}}}\mu_{\text{ref}}, \quad (1)$$

using  $^{210}\text{Fr}$  [ $I_{\text{ref}} = 6^+$ ,  $\mu_{\text{ref}} = +4.38(5)\mu_N$ ,  $A_{\text{ref}}(7s^2S_{1/2}) = +7195.9(9)$  MHz] as a reference [13,31]. Only the  $A$  factor for the lower-state  $7s^2S_{1/2}$  splitting was used to calculate the magnetic moment, due to its smaller relative uncertainty. The 1% error on the magnetic moments of  $^{203,207}\text{Fr}$  is dominated by the error on the reference value  $\mu(^{210}\text{Fr})$ . This is of the same order as the hyperfine anomaly that was observed between odd- $A$  and even- $A_{87}\text{Fr}$  isotopes [32].

The spectroscopic quadrupole moments were calculated by using theoretical calculations of the electric-field gradient, since there are no experimentally determined values for this quantity. Coupled-cluster many-body calculations from Ref. [30] give

$$\frac{B(8p^2P_{3/2})}{Q_s} = +84.01 \text{ MHz/b}, \quad (2)$$

allowing the spectroscopic quadrupole moment to be obtained. The uncertainty on the measured quadrupole moment derives only from the statistical error on  $B(8p^2P_{3/2})$  because no error is given for the calculated quantity in Eq. (2). To ensure consistency when comparing quadrupole moments obtained through different transitions, literature values from Refs. [13,19] measured with the 718 nm transition have been reevaluated by using

$$\frac{B(7p^2P_{3/2})}{Q_s} = +259.73 \text{ MHz/b}, \quad (3)$$

also calculated in Ref. [30]. No additional error was added to the quadrupole moments as the calculations presented in Ref. [30] agree with experimental data of hyperfine  $B$  factors for the  $7p^2P_{3/2}$  and  $8p^2P_{3/2}$  states in both  $^{210,212}\text{Fr}$ .

Changes in mean-square charge-radii were calculated by using

$$\delta\langle r^2 \rangle^{A,A'} = \frac{1}{F_{422}} \left( \delta\nu^{A,A'} - M_{422} \frac{A' - A}{AA'} \right), \quad (4)$$

with  $M_{422} = +750(330)$  GHz amu and  $F_{422} = -20.67(21)$  GHz/ $\text{fm}^2$  as detailed in our earlier work [15]. Both statistical and systematic errors are quoted for the changes in mean-square charge radii. The statistical error results from the experimental error on the isotope shift and the systematic error arises from the uncertainty on the atomic  $M$  and  $F$  factors.

#### IV. DISCUSSION

The measured hyperfine  $A$  factors and isotope shifts for  $^{203,207}\text{Fr}$  agree with literature values [13,15,16]. The uncertainty on  $A(7s^2S_{1/2})$  and  $\delta\nu^{221,A}$  for  $^{203}\text{Fr}$  has improved by an order of magnitude. Despite this reduction, the precision on the magnetic moment of  $^{203}\text{Fr}$  has not improved because the uncertainty is dominated by the reference value. The statistical uncertainty on the relative charge radius of  $^{203}\text{Fr}$  has decreased by an order of magnitude and this strengthens the earlier suggested departure from the  $_{82}\text{Pb}$  chain [16].

The spectroscopic quadrupole moments for even- $N$   $_{87}\text{Fr}$  isotopes below the  $N = 126$  shell closure are shown in Fig. 2. Literature values are taken from Refs. [12,13]. In the extreme single-particle spherical shell model, even- $N$   $_{87}\text{Fr}$  isotopes are expected to have quadrupole moments equal to zero because the  $\pi 1h_{9/2}$  orbital is half filled [23]. The fact that the measured quadrupole moments are nonzero indicates some degree of core polarization.

The quadrupole moments between  $N = 118$ –126 seem to follow a linear trend (as shown by the dashed line to guide the eye). A departure from this trend occurs at  $^{203}\text{Fr}$ , suggesting a possible onset of static deformation which is larger than the normal “core polarization.” A deviation from the literature value of  $^{207}\text{Fr}$  can be seen in the new measurement, reducing its uncertainty and bringing it more in line with the systematics of the region.

An increase in the magnitude of the quadrupole moments of  $\pi h_{9/2}^n$  configurations with increasing number of neutron holes in the  $N = 126$  shell has been observed in all isotope and isomers up to  $_{88}\text{Ra}$  [23]. Previously, a parabolic trend was fit to the available data to extrapolate the effective proton charge at  $N = 114$  [ $e_{\pi}^{\text{emp}}(N = 114)/e_{\pi}^{\text{emp}}(N = 126) = 2.42$ ], as detailed in Ref. [23]. With the recent and present data on the  $_{87}\text{Fr}$  ground

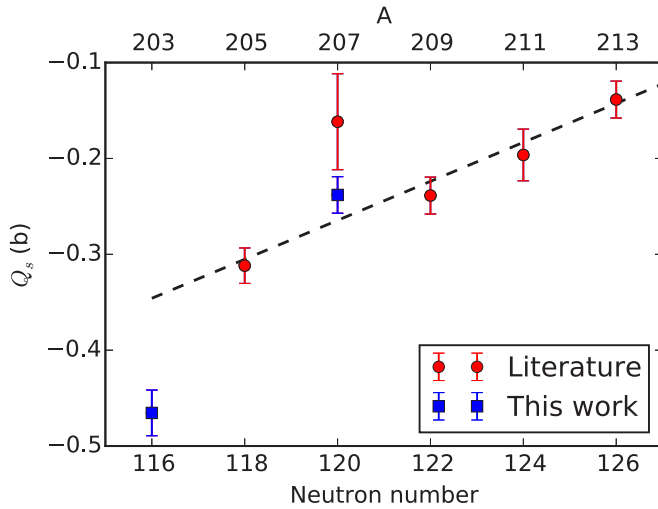


FIG. 2. Spectroscopic quadrupole moments of even- $N$   $_{87}\text{Fr}$  isotopes below the  $N = 126$  shell closure. This work is shown in blue squares, literature values are shown in red circles [12,13]. A linear fit of the data between  $N = 118$ – $126$  is shown as a dashed line.

states [12,13] probing a rather pure  $\pi h_{9/2}^5$  configuration, the proposed parabolic behavior can be further tested. A similar plot is presented in Fig. 3, displaying only the  $8^+$  states in  $_{84}\text{Po}$ , and the  $9/2^-$  states in  $_{83}\text{Bi}$  and  $_{87}\text{Fr}$ , for clarity. Note that, because the  $_{83}\text{Bi}$  and  $_{87}\text{Fr}$  measurements were obtained through laser spectroscopy, the ratio of the quadrupole moments is equal to the ratio of the measured hyperfine  $B$  factors and is thus independent of any electric-field-gradient calibration. Because the literature values of the  $_{87}\text{Fr}$  quadrupole moments were obtained from a different atomic state, the theoretical  $B(7p^2P_{3/2})/B(8p^2P_{3/2}) = 3.09$  scaling factor from Ref. [30] was used to determine the normalized quadrupole moments.

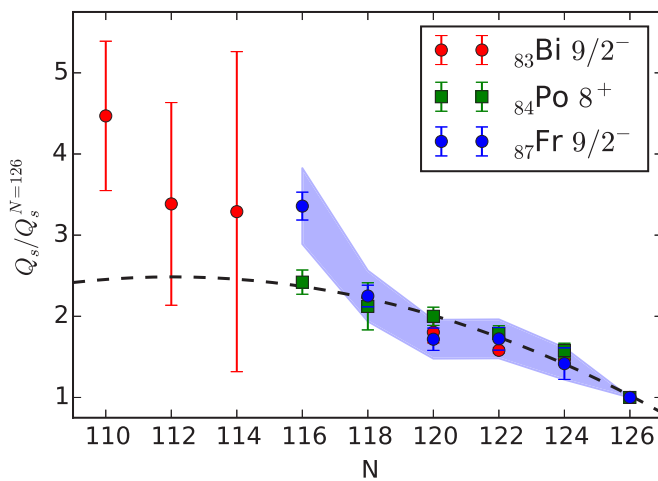


FIG. 3. The ratio of quadrupole moments below  $N = 126$  to the quadrupole moment at  $N = 126$  for the  $9/2^-$  ground states in  $_{83}\text{Bi}$  (red circles) [10],  $_{87}\text{Fr}$  (blue squares) [12,13], and  $8^+$  states in  $_{84}\text{Po}$  (green triangles) [33]. The shaded area indicates the contribution of the  $Q_s(^{213}\text{Fr})$  uncertainty on the ratio. The dashed line results from a quadratic fit of all data. See text for details.

TABLE II. Intrinsic quadrupole moment and calculated static and total deformation parameters for  $^{203}\text{Fr}$ .

A	$Q_0$ (b)	$ \langle\beta_2\rangle $	$\langle\beta_2\rangle_{\text{tot}}$	Ratio (%)
203	-0.85(4)	0.026(1)	0.118(2)	22(1)

This scaling factor agrees perfectly with the experimentally determined ratio  $B(7p^2P_{3/2})/B(8p^2P_{3/2}) = 3.08(6)$  [11–13,34]. The shaded area on the  $_{87}\text{Fr}$  data represents the error on the quadrupole-moment ratios due to the error of the  $^{213}\text{Fr}$  reference quadrupole moment. Such an error is not shown for the  $_{83}\text{Bi}$  and  $_{84}\text{Po}$  data because it is negligible compared with the total uncertainty on the normalized quadrupole moment. The quadratic fit, shown by the dashed line in Fig. 3, is fit to the same data as in Ref. [23] but also includes the  $9/2^-$  states in  $_{87}\text{Fr}$  (down to  $^{205}\text{Fr}$  [12,13]) and the  $8^+$  states in  $_{88}\text{Ra}$  [35]. The  $_{83}\text{Bi}$  data for  $N = 110$ – $114$  are not included. The empirically derived effective proton charge of  $e_{\pi}^{\text{emp}}(N = 114)/e_{\pi}^{\text{emp}}(N = 126) = 2.46(14)$  presented here is in good agreement with the value derived in Ref. [23].

The normalized quadrupole moments of the  $_{83}\text{Bi}$ ,  $_{84}\text{Po}$ , and  $_{87}\text{Fr}$  isotopes follow a very similar trend, down to  $N = 118$ , despite their different proton numbers. The enhancement in quadrupole collectivity with decreasing neutron number is attributed to enhanced proton-neutron correlations as more neutron-holes appear beneath  $N = 126$  and seems to be independent of the proton configuration for a given state. This steady increase of core polarization begins to saturate as  $N$  decreases. The  $_{87}\text{Fr}$  isotopic chain shows the earliest clear deviation from this trend, at  $^{203}\text{Fr}$ . This suggests a sudden onset of static deformation (contrary to the gradual onset of core polarization) from  $N = 116$  downwards. A deviation from the trend also occurs in  $_{83}\text{Bi}$ , six neutrons closer to the midshell region.

Table II shows the intrinsic quadrupole moment and calculated static and total deformation parameters for  $^{203}\text{Fr}$ . The intrinsic quadrupole moment  $Q_0$  was calculated in the strong-coupling limit by using

$$Q_0 = \frac{(I+1)(2I+3)}{I(2I-1)} Q_s. \quad (5)$$

The static deformation parameter  $|\langle\beta_2\rangle|$  was calculated from the intrinsic quadrupole moment with

$$Q_0 = \frac{5Z\langle r^2 \rangle_{\text{sph}}}{\sqrt{5\pi}} \langle\beta_2\rangle (1 + 0.36\langle\beta_2\rangle), \quad (6)$$

by using the second parametrization of the liquid-droplet model presented in Ref. [36] for  $\langle r^2 \rangle_{\text{sph}}$ . The total deformation parameter  $\langle\beta_2\rangle_{\text{tot}}$  was deduced from the relative charge radius of  $^{203}\text{Fr}$  by using the same parametrization of the liquid-droplet model fixing  $\langle\beta\rangle_{\text{tot}}(^{213}\text{Fr}) = \langle\beta\rangle_{\text{tot}}(^{212}\text{Rn}) = 0.062$  [37]. Despite the sudden increase in the quadrupole moment in this nucleus, the static deformation comprises only 22(1)% of the total nuclear deformation. Therefore,  $^{203}\text{Fr}$  cannot be considered as purely statically deformed and the increase in quadrupole deformation cannot fully account for the departure of its relative charge radius from the  $_{82}\text{Pb}$  chain [16], indicating

the presence of other effects. In  $^{84}\text{Po}$ , the onset of ground-state deformation was interpreted in the beyond-mean-field picture to be due to an increased admixture of deformed configurations [21]. Theoretical input would help clarify the origin of deformation in neutron deficient  $^{87}\text{Fr}$ .

Measurements of the changes in mean-square charge radii of neutron-deficient  $^{83}\text{Bi}$  isotopes show a departure from the neighboring  $^{82}\text{Pb}$  chain at  $N = 110$  [20], suggesting an onset of deformation. However, the missing quadrupole moment data for  $N = 116, 118$  and the low-precision data for  $N = 110\text{--}114$  prevent firm conclusions on the nature of this deformation in the  $^{83}\text{Bi}$  isotopic chain. High-resolution laser spectroscopy measurements for  $N < 120$  are required to determine its nature and confirm the neutron number at which the deviation occurs compared with  $^{87}\text{Fr}$ .

## V. CONCLUSION

High-resolution collinear resonance ionization spectroscopy was performed on neutron-deficient francium, allowing the measurement of the spectroscopic quadrupole moment of  $^{203}\text{Fr}$ . With a linewidth of 25 MHz, the hyperfine structures of  $^{203,207}\text{Fr}$  were probed, providing hyperfine  $A$  and  $B$  factors of the atomic state  $8p^2P_{3/2}$ , in addition to more precise isotope shifts. A more accurate measurement of the quadrupole moment of  $^{207}\text{Fr}$  deviates from the literature value but is more in agreement with the systematic trend observed in the region. The normalized quadrupole moments of the even- $N$   $^{87}\text{Fr}$  isotopes were compared with those of other ground and isomeric states in the trans-lead region. All these quadrupole moments follow the same quadratic increase with decreasing neutron number, irrespective of their proton

configuration, down to  $N = 118$ .  $^{203}\text{Fr}$ , at  $N = 116$ , is the first isotope for which a clear deviation is seen from this trend, suggesting an onset of static deformation in the  $^{87}\text{Fr}$  isotopes at  $N = 116$ . However, calculations of the static and total deformation parameters show that  $^{203}\text{Fr}$  is not a purely statically deformed nucleus. The increase in quadrupole deformation in this nucleus cannot fully account for the observed departure of its relative charge radius from its  $^{82}\text{Pb}$  isotone. Further measurements approaching the midshell are needed to see if the ground states become statically deformed or if their deformation is due to configuration mixing with deformed states as in  $^{84}\text{Po}$  [21]. High-resolution laser spectroscopy studies on neutron deficient  $^{83}\text{Bi}$  are needed to verify whether a similar onset of ground-state static deformation occurs at  $N = 110$ , as is suggested in Ref. [20].

## ACKNOWLEDGMENTS

We acknowledge the support of the ISOLDE collaboration and technical teams. This work was supported by ERC Consolidator Grant No. 648381; the Science and Technology Facilities Council Consolidated Grant No. ST/F012071/1, Continuation Grant No. ST/J000159/1, and Ernest Rutherford Grant No. ST/L002868/1; the IUAP-Belgian State Belgian Science Policy (BRIX network P7/12), FWO-Vlaanderen (Belgium) and GOA 15/010 from KU Leuven; and the European Union Seventh Framework Programme for Research and Technological Development under Grant Agreements No. 262010 (ENSAR), No. 267194 (COFUND), and No. 289191 (LA3NET). We acknowledge financial aid from the Ed Schneiderman Fund at New York University.

- 
- [1] K. Heyde and J. L. Wood, *Rev. Mod. Phys.* **83**, 1467 (2011).
- [2] C. N. Davids, P. J. Woods, H. T. Penttilä, J. C. Batchelder, C. R. Bingham, D. J. Blumenthal, L. T. Brown, B. C. Busse, L. F. Conticchio, T. Davinson, D. J. Henderson, R. J. Irvine, D. Seweryniak, K. S. Toth, W. B. Walters, and B. E. Zimmerman, *Phys. Rev. Lett.* **76**, 592 (1996).
- [3] H. Kettunen, T. Enqvist, M. Leino, K. Eskola, P. Greenlees, K. Helariutta, P. Jones, R. Julin, S. Juutinen, H. Kankaanpää, H. Koivisto, P. Kuusiniemi, M. Muikku, P. Nieminen, P. Rahkila, and J. Uusitalo, *Eur. Phys. J. A* **16**, 457 (2003).
- [4] U. Jakobsson, J. Uusitalo, S. Juutinen, M. Leino, T. Enqvist, P. T. Greenlees, K. Hauschild, P. Jones, R. Julin, S. Ketelhut, P. Kuusiniemi, M. Nyman, P. Peura, P. Rahkila, P. Ruotsalainen, J. Sarén, C. Scholey, and J. Sorri, *Phys. Rev. C* **85**, 014309 (2012).
- [5] U. Jakobsson, S. Juutinen, J. Uusitalo, M. Leino, K. Auranen, T. Enqvist, P. T. Greenlees, K. Hauschild, P. Jones, R. Julin, S. Ketelhut, P. Kuusiniemi, M. Nyman, P. Peura, P. Rahkila, P. Ruotsalainen, J. Sarén, C. Scholey, and J. Sorri, *Phys. Rev. C* **87**, 054320 (2013).
- [6] U. Jakobsson, J. Uusitalo, K. Auranen, H. Badran, B. Cederwall, D. M. Cox, T. Grahn, P. T. Greenlees, R. Julin, S. Juutinen, A. Herzán, J. Konki, M. Leino, M. Mallaburn, J. Pakarinen, P. Papadakis, J. Partanen, P. Rahkila, M. Sandzelius, J. Sareñ, C. Scholey, J. Sorri, and S. Stolze, *Nuc. Phys. Rev.* **33**, 141 (2016).
- [7] Z. Kalaninová, A. N. Andreyev, S. Antalic, F. P. Heßberger, D. Ackermann, B. Andel, M. C. Drummond, S. Hofmann, M. Huyse, B. Kindler, J. F. W. Lane, V. Liberati, B. Lommel, R. D. Page, E. Rapisarda, K. Sandhu, Š. Šáro, A. Thornthwaite, and P. Van Duppen, *Phys. Rev. C* **87**, 044335 (2013).
- [8] A. E. Barzakh, D. V. Fedorov, V. S. Ivanov, P. L. Molkanov, F. V. Moroz, S. Y. Orlov, V. N. Pantelev, M. D. Seliverstov, and Y. M. Volkov, *Phys. Rev. C* **94**, 024334 (2016).
- [9] H. De Witte, A. N. Andreyev, N. Barré, M. Bender, T. E. Cocolios, S. Dean, D. Fedorov, V. N. Fedoseyev, L. M. Fraile, S. Franchoo, V. Hellemans, P. H. Heenen, K. Heyde, G. Huber, M. Huyse, H. Jeppessen, U. Köster, P. Kunz, S. R. Leshner, B. A. Marsh, I. Mukha, B. Roussière, J. Sauvage, M. Seliverstov, I. Stefanescu, E. Tengborn, K. Van de Vel, J. Van de Walle, P. Van Duppen, and Y. Volkov, *Phys. Rev. Lett.* **98**, 112502 (2007).
- [10] M. R. Pearson, P. Campbell, K. Leerungnavarat, J. Billowes, I. S. Grant, M. Keim, J. Kilgallon, I. D. Moore, R. Neugart, M. Neuroth, S. Wilbert, and the ISOLDE Collaboration, *J. Phys. G* **26**, 1829 (2000).
- [11] K. M. Lynch, T. E. Cocolios, J. Billowes, M. L. Bissell, I. Budinčević, T. D. Goodacre, R. P. de Groote, G. J. Farooq-Smith, V. N. Fedosseev, K. T. Flanagan, S. Franchoo, R. F. G. Ruiz, H. Heylen, R. Li, B. A. Marsh, G. Neyens, R. E. Rossel, S. Rothe, H. H. Stroke, K. D. A. Wendt, S. G. Wilkins, and X. Yang, *Phys. Rev. C* **93**, 014319 (2016).

- [12] A. Voss, F. Buchinger, B. Cheal, J. E. Crawford, J. Dilling, M. Kortelainen, A. A. Kwiatkowski, A. Leary, C. D. P. Levy, F. Mooshammer, M. L. Ojeda, M. R. Pearson, T. J. Procter, and W. A. Tamimi, *Phys. Rev. C* **91**, 044307 (2015).
- [13] A. Coc, C. Thibault, F. Touchard, H. Duong, P. Juncar, S. Liberman, J. Pinard, J. Lermé, J. Vialle, S. Büttgenbach, A. Mueller, and A. Pesnelle, *Phys. Lett. B* **163**, 66 (1985).
- [14] R. P. de Groote, I. Budinčević, J. Billowes, M. L. Bissell, T. E. Cocolios, G. J. Farooq-Smith, V. N. Fedosseev, K. T. Flanagan, S. Franchoo, R. F. G. Ruiz, H. Heylen, R. Li, K. M. Lynch, B. A. Marsh, G. Neyens, R. E. Rossel, S. Rothe, H. H. Stroke, K. D. A. Wendt, S. G. Wilkins, and X. F. Yang, *Phys. Rev. Lett.* **115**, 132501 (2015).
- [15] K. M. Lynch, J. Billowes, M. L. Bissell, I. Budinčević, T. E. Cocolios, R. P. De Groote, S. De Schepper, V. N. Fedosseev, K. T. Flanagan, S. Franchoo, R. F. G. Ruiz, H. Heylen, B. A. Marsh, G. Neyens, T. J. Procter, R. E. Rossel, S. Rothe, I. Strashnov, H. H. Stroke, and K. D. A. Wendt, *Phys. Rev. X* **4**, 011055 (2014).
- [16] K. T. Flanagan, K. M. Lynch, J. Billowes, M. L. Bissell, I. Budinčević, T. E. Cocolios, R. P. de Groote, S. De Schepper, V. N. Fedosseev, S. Franchoo, R. F. G. Ruiz, H. Heylen, B. A. Marsh, G. Neyens, T. J. Procter, R. E. Rossel, S. Rothe, I. Strashnov, H. H. Stroke, and K. D. A. Wendt, *Phys. Rev. Lett.* **111**, 212501 (2013).
- [17] G. J. Farooq-Smith, T. E. Cocolios, J. Billowes, M. L. Bissell, I. Budinčević, T. D. Goodacre, R. P. de Groote, V. N. Fedosseev, K. T. Flanagan, S. Franchoo, R. F. G. Ruiz, H. Heylen, R. Li, K. M. Lynch, B. A. Marsh, G. Neyens, R. E. Rossel, S. Rothe, H. H. Stroke, K. D. A. Wendt, S. G. Wilkins, and X. F. Yang, *Phys. Rev. C* **94**, 054305 (2016).
- [18] I. Budinčević, J. Billowes, M. L. Bissell, T. E. Cocolios, R. P. de Groote, S. De Schepper, V. N. Fedosseev, K. T. Flanagan, S. Franchoo, R. F. G. Ruiz, H. Heylen, K. M. Lynch, B. A. Marsh, G. Neyens, T. J. Procter, R. E. Rossel, S. Rothe, I. Strashnov, H. H. Stroke, and K. D. A. Wendt, *Phys. Rev. C* **90**, 014317 (2014).
- [19] A. Voss, M. R. Pearson, J. Billowes, F. Buchinger, B. Cheal, J. E. Crawford, A. A. Kwiatkowski, C. D. P. Levy, and O. Shelbaya, *Phys. Rev. Lett.* **111**, 122501 (2013).
- [20] A. E. Barzakh, D. V. Fedorov, V. S. Ivanov, P. L. Molkanov, F. V. Moroz, S. Y. Orlov, V. N. Panteleev, M. D. Seliverstov, and Y. M. Volkov, *Phys. Rev. C* **95**, 044324 (2017).
- [21] T. E. Cocolios, W. Dexters, M. D. Seliverstov, A. N. Andreyev, S. Antalic, A. E. Barzakh, B. Bastin, J. Büscher, I. G. Darby, D. V. Fedorov, V. N. Fedosseev, K. T. Flanagan, S. Franchoo, S. Fritzsche, G. Huber, M. Huyse, M. Keupers, U. Köster, Y. Kudryavtsev, E. Mané, B. A. Marsh, P. L. Molkanov, R. D. Page, A. M. Sjoedin, I. Stefan, J. Van de Walle, P. Van Duppen, M. Venhart, S. G. Zemlyanoy, M. Bender, and P.-H. Heenen, *Phys. Rev. Lett.* **106**, 052503 (2011).
- [22] M. Seliverstov, T. Cocolios, W. Dexters, A. Andreyev, S. Antalic, A. Barzakh, B. Bastin, J. Büscher, I. Darby, D. Fedorov, V. Fedosseev, K. Flanagan, S. Franchoo, S. Fritzsche, G. Huber, M. Huyse, M. Keupers, U. Köster, Y. Kudryavtsev, B. Marsh, P. Molkanov, R. Page, A. M. Sjoedin, I. Stefan, J. Van de Walle, P. V. Duppen, M. Venhart, and S. Zemlyanoy, *Phys. Lett. B* **719**, 362 (2013).
- [23] G. Neyens, *Rep. Prog. Phys.* **66**, 633 (2003).
- [24] E. Mané, J. Billowes, K. Blaum, P. Campbell, B. Cheal, P. Delahaye, K. Flanagan, D. Forest, H. Franberg, C. Geppert, T. Giles, A. Jokinen, M. Kowalska, R. Neugart, G. Neyens, W. Nörtershäuser, I. Podadera, G. Tungate, P. Vingerhoets, and D. Yordanov, *Eur. Phys. J. A* **42**, 503 (2009).
- [25] T. E. Cocolios, H. H. A. Suradi, J. Billowes, I. Budinčević, R. P. de Groote, S. D. Schepper, V. N. Fedosseev, K. T. Flanagan, S. Franchoo, R. F. G. Ruiz, H. Heylen, F. L. Blanc, K. M. Lynch, B. A. Marsh, P. J. R. Mason, G. Neyens, J. Papuga, T. J. Procter, M. M. Rajabali, R. E. Rossel, S. Rothe, G. S. Simpson, A. J. Smith, I. Strashnov, H. H. Stroke, D. Verney, P. M. Walker, K. D. A. Wendt, and R. T. Wood, *Nucl. Instrum. Methods Phys. Res., Sect. B* **317**, Part B, 565 (2013).
- [26] R. P. de Groote, K. M. Lynch, and S. G. Wilkins, *Hyperfine Interact.* **238**, 5 (2016).
- [27] S. Aubin, E. Gomez, L. A. Orozco, and G. D. Sprouse, *Phys. Rev. A* **70**, 042504 (2004).
- [28] R. P. de Groote, M. Verlinde, V. Sonnenschein, K. T. Flanagan, I. Moore, and G. Neyens, *Phys. Rev. A* **95**, 032502 (2017).
- [29] V. A. Dzuba, W. R. Johnson, and M. S. Safronova, *Phys. Rev. A* **72**, 022503 (2005).
- [30] B. K. Sahoo, D. K. Nandy, B. P. Das, and Y. Sakemi, *Phys. Rev. A* **91**, 042507 (2015).
- [31] E. Gomez, S. Aubin, L. A. Orozco, G. D. Sprouse, E. Iskrenova-Tchoukova, and M. S. Safronova, *Phys. Rev. Lett.* **100**, 172502 (2008).
- [32] J. Zhang, M. Tandecki, R. Collister, S. Aubin, J. A. Behr, E. Gomez, G. Gwinner, L. A. Orozco, M. R. Pearson, and G. D. Sprouse, *Phys. Rev. Lett.* **115**, 042501 (2015).
- [33] G. Neyens, S. Ternier, N. Coulier, K. Vyvey, R. Coussement, and D. Balabanski, *Nucl. Phys. A* **625**, 668 (1997).
- [34] H. T. Duong, P. Juncar, S. Liberman, A. C. Mueller, R. Neugart, E. W. Otten, B. Peuse, J. Pinard, H. H. Stroke, C. Thibault, F. Touchard, J. L. Vialle, K. Wendt, and ISOLDE Collaboration, *Europhys. Lett.* **3**, 175 (1987).
- [35] G. Neyens, R. Nouwen, G. S'heeren, M. V. D. Bergh, and R. Coussement, *Nucl. Phys. A* **555**, 629 (1993).
- [36] D. Berdichevsky and F. Tondeur, *Z. Phys. A: At. Nucl.* (1975) **322**, 141 (1985).
- [37] S. Raman, C. W. Nestor, and P. Tikkanen, *At. Data Nucl. Data Tables* **78**, 1 (2001).